

# Short-term evolution and coexistence of spots, plages and flare activity on LQ Hydrae<sup>★</sup>

M. Flores Soriano and K. G. Strassmeier

Leibniz-Institut für Astrophysik Potsdam (AIP), An der Sternwarte 16, 14482 Potsdam, Germany  
e-mail: [mflores;kstrassmeier@aip.de]

Received ...; Accepted...

## Abstract

**Aims.** We aim to study the short-term evolution of the chromospheric and photospheric activity of the young, single K2 dwarf LQ Hya. **Methods.** Four months of quasi-simultaneous spectroscopic and photometric observations were used to study the variations of the photometric light curve, the evolution of the chromospheric activity from the H $\alpha$  and H $\beta$  lines, and the distribution of cool spots from Doppler maps.

**Results.** During our observations one side of the star was more active than the other. The equivalent width of the H $\alpha$  line from the least active hemisphere increased from  $\approx 0.7 \text{ \AA}$  at the beginning of the observation to  $1.0 \text{ \AA}$  at the end. The basal emission of the most active hemisphere remained roughly constant at  $EW_{H\alpha} \approx 1.0 \text{ \AA}$ . Intense flare activity was observed during the first twenty days, where at least four different events were detected. The line asymmetries of the H $\alpha$  line suggest that one of the flares could have produced a mass ejection with a maximum projected speed of  $70 \text{ km s}^{-1}$ . The rotational modulation of the V-band photometry showed clear anti-correlation with the chromospheric activity. The difference in brightness between the opposite hemispheres decreased from  $0^{\text{m}}16$  to  $0^{\text{m}}09$  in two months. Three spots gradually moving apart from each other are dominating the photospheric Doppler maps. The comparison between the maps and the H $\alpha$  line as the star rotates reveals the spatial coexistence of chromospheric H $\alpha$  emission and photospheric spots.

**Conclusions.** Our results indicate that the active regions of LQ Hya can live for at least four months. The detected changes in the photometric light curve and the spectroscopic Doppler images seem to be more a consequence of the spatial redistribution of the active regions rather than due to changes in their strength. Only one of the active regions shows significant changes in its chromospheric emission.

**Key words.** stars: activity - stars: chromospheres - stars: evolution - stars: flare - stars: imaging - stars: individual: LQ Hydrae

## 1. Introduction

LQ Hya (HD 82558) is a young, single, fast rotating K2 dwarf with high magnetic activity. It was first identified as a chromospherically active star by the surveys of [Bidelman \(1981\)](#) and [Heintz \(1981\)](#). [Fekel et al. \(1986b\)](#) observed the H $\alpha$  line completely filled-in by emission and classified the star as a BY Draconis variable. Age estimations suggest that the star could probably have just arrived on the zero-age main sequence. From its fast rotation and high lithium abundance, [Fekel et al. \(1986a\)](#) concluded that LQ Hya is not older than 75 Myr, “at least as young as the youngest Pleiades star”. The lack of persistent variability in the radial velocity of LQ Hya indicates that it is a single star (see, e.g., [Fekel et al. 1986a](#); [Donati et al. 2003](#)). Nonetheless, occasional rotational modulations produced by asymmetric spot distributions have also been observed ([Flores Soriano et al. 2015](#), hereafter [Paper I](#)).

Because of its physical properties, LQ Hya is commonly considered a young solar-like star, and a good link between the very active and fast rotating pre-main sequence stars and the more evolved stars from the main sequence that have already undergone rotational momentum loss. It has been the target of numerous photometric studies. The rotational modulation of its

light curve indicates that the star rotates with a period of  $P_{\text{rot}} \approx 1.6 \text{ d}$ . With data available since the early 1980s, many authors have found signs of periodic spot activity in three time ranges: a short cycle with a period between 2 and 3 yr ([Oláh & Strassmeier 2002](#); [Messina & Guinan 2003](#); [Kővári et al. 2004](#); [Oláh et al. 2009](#); [Lehtinen et al. 2016](#)), an intermediate cycle with a period in the range 6-7 yr ([Jetsu 1993](#); [Strassmeier et al. 1997a](#); [Oláh et al. 2000](#); [Berdyugina et al. 2002](#); [Messina & Guinan 2003](#); [Kővári et al. 2004](#)), and a longer cycle with a 11-18 yr period ([Oláh et al. 2000](#); [Berdyugina et al. 2002](#); [Messina & Guinan 2003](#); [Kővári et al. 2004](#); [Lehtinen et al. 2012](#); [Lehtinen et al. 2016](#)). [Berdyugina et al. \(2002\)](#) found that two active longitudes dominated the activity over 20 years and reported an additional 5.2 yr flip-flop cycle. On the contrary, [Lehtinen et al. \(2012\)](#) and [Olsperg et al. \(2015\)](#) have not found any periodicity for this kind of events. Coherent active longitudes were found by [Lehtinen et al. \(2016\)](#) only between 2003 and 2008. The time scale of the changes in the light curve has been reported to be of a few months by [Jetsu \(1993\)](#) and 50.5 d by [Lehtinen et al. \(2012\)](#).

The star is also known for being chromospherically active. [Strassmeier et al. \(1993\)](#), [Frasca et al. \(2008\)](#), [Cao & Gu \(2014\)](#), and [Paper I](#) found a clear anti-correlation between the rotational modulation of the chromospheric emission and the photometric light curve. This points out the spatial connection between photospheric dark spots, and chromospheric plages and possibly microflare activity (see [Paper I](#) for a characterization of the emission sources). In addition to this, [Cao & Gu \(2014\)](#) also found

<sup>★</sup> Based on data obtained with the STELLA robotic telescope in Tenerife, an AIP facility jointly operated by AIP and IAC, and the Vienna-Potsdam Automatic Photoelectric Telescopes at Fairborn Observatory in Arizona, operated by AIP.

that the chromospheric activity gradually decreased from 2006 to 2012, which corresponds to a period of constant increment in the average brightness of the star (Lehtinen et al. 2016).

Strong flares have been reported in LQ Hya in different wavelengths. Ambruster & Fekel (1990) detected an UV flare, but curiously without enhancement in the chromospheric lines. On the other hand, Montes et al. (1999) observed a flare in both optical and UV wavelengths, but with the optical flare apparently delayed. They found that the chromospheric lines reached their maximum intensity  $\approx 55$  min after the impulsive phase. Covino et al. (2001) observed an X-ray flare and derived a loop semi-length of  $\approx 1.5$  stellar radii. Frequent low-level flare activity was also reported by Saar & Bookbinder (1998) and in Paper I.

LQ Hya has been regularly analyzed with surface mapping techniques since the early 1990s (Saar et al. 1992; Strassmeier et al. 1993; Saar et al. 1994; Rice & Strassmeier 1998). Nearly annual magnetic and brightness maps were computed by Donati (1999) and Donati et al. (2003) for the period 1991 - 2001. Their brightness images usually show a polar spot and some low latitude spots, but with clear changes in the configuration from one year to the next. Berdyugina et al. (2001) computed temperature maps from 1993 to 1999 with a typical time interval between images of about four months. They reported a rapid evolution of the active regions, on a time scale of months. Kóvári et al. (2004) reconstructed 28 maps from 35 consecutive stellar rotations and saw rapid spot evolution on time scales from 1 day to 20 days. They interpreted the fast changes in the spot configuration as due to magnetic reconnection rather than due to spot migration or the emergence of new flux tubes. More recently, Cole et al. (2015) computed seven maps for the observing seasons 1998 – 2002. They addressed a chaotic spot activity but apparently concentrated at two latitudes.

In spite of all this progress, the short term evolution of the magnetic activity of LQ Hya remains puzzling. Studies based on spectral data are usually either from observing campaigns that are not long enough to show any significant change, or from interseasonal data that are too sparse to follow the evolution of individual magnetic regions. In Paper I we analyzed a time series of 199 LQ Hya spectra and quasi-simultaneous photometry to study the rotational modulation of chromospheric and photospheric parameters and their connection with the variability of the LiI 6708 Å line. We found that during the four months of nearly continuous observations the star presented a relatively stable activity configuration, where one side of the star was clearly more active than the other. In this paper we use the superior spectral time coverage of those observations to study the temporal evolution of the magnetic activity of LQ Hya in a previously unexplored timescale. Sect. 2 describes our data and observations. The temporal evolution of the chromospheric emission at different phases is presented in Sect. 3. The photospheric variability is analyzed in Sect. 4 with photometry and by means of Doppler imaging. Sect. 5 combines our results and explores the connection between the photospheric spots and the chromospheric activity. Finally, Sect. 6 summarizes and concludes the paper.

## 2. Observations and data reduction

### 2.1. STELLA/SES spectroscopy

For this work we used the same spectroscopic data as in Paper I. They are a time series of 199 echelle spectra taken between December 2011 and April 2012 with the STELLA Echelle Spectrograph (SES) at the robotic 1.2 m STELLA-I telescope at the Observatorio del Teide in Tenerife, Spain (Strassmeier

et al. 2010). The integration time was set to 3600 s, providing signal-to-noise ratios (S/N) between 40 and 120. During the observations the spectrograph covered the wavelength range from 476 to 764 nm with a resolving power of  $R = 30\,000$ . The SES spectrograph normally operates with a fixed spectral range of 388–882 nm and  $R = 55\,000$ . However, our observations were made during an interruption in the ongoing spectrograph upgrade. At that time the collimator was slightly misaligned and the old camera out of focus, which caused the shorter spectral range and the significantly lower spectral resolution. For more details about the instruments and data reduction we refer to Paper I and references therein.

### 2.2. Amadeus APT photometry

Quasi-simultaneously to the STELLA observations, phase-resolved V-band photometry was obtained with the 0.75 m Potsdam-APT *Amadeus* (T7) telescope at Fairborn Observatory in southern Arizona (Strassmeier et al. 1997b). They are basically the same data as in Paper I, but we have added new values to improve the time and phase coverage of our evolution analysis. The total amount of measurements is now 1144. All measurements were made differentially with respect to HD 82447 and HD 82508 as the comparison and check star, respectively. The integration time was 10 s. Data taken before 2012-02-20 are affected by instrumental problems. They are substantially more disperse and have larger error bars. Most of these values have been removed and only those of apparently better quality are kept. For further details about the observing procedure and the APT data reduction, we refer to Granzer et al. (2001). The uncertainties were calculated as indicated in Hall et al. (1986).

## 3. Evolution of the H $\alpha$ and H $\beta$ chromospheric emission

In Paper I we studied the rotational modulation of the chromospheric activity of LQ Hya from the emission of the Balmer H $\alpha$  and H $\beta$  lines. We evaluated the equivalent widths (EWs) of the net emission profiles by integrating the spectra resulting from the subtraction of a non-active template. We found that the chromospheric emission in these lines can be divided into two different types of contributions. The first contribution is a relatively stable emission with H $\alpha$  EWs in the range 0.7 – 1.2 Å that we attributed to a combination of plages and repeated low-intensity flares. It is rotationally modulated and presents maximum values when the most spotted side of the star is in view. The other contribution consists in more energetic episodes ( $EW_{H\alpha} \gtrsim 1.2$  Å) that correspond to sporadic flares of moderate intensity, occurring predominantly also on the most spotted side of the star. In this section we will discuss the temporal evolution of these chromospheric emissions. As the H $\alpha$  and H $\beta$  lines present a similar behavior, we will focus our analysis on the variations of the H $\alpha$  line. The numerical values of the EWs of both lines, their associated radiative flux, and the Balmer decrements  $F_{H\alpha}/F_{H\beta}$  are available at the online material of Paper I<sup>1</sup>.

<sup>1</sup> Available at the CDS via anonymous ftp to [cdsarc.u-strasbg.fr\(130.79.128.5\)](http://cdsarc.u-strasbg.fr(130.79.128.5)) or via <http://cdsarc.u-strasbg.fr/viz-bin/qcat?J/A+A/575/A57>

### 3.1. Sporadic flare emission

The top panel of Figure 1 shows the EW of the  $H\alpha$  line for each one of the 199 LQ Hya spectra at different times and phases. As in Paper I, we phased the observations with the ephemeris  $HJD = HJD_0 + 1.60066 \cdot E$ , where the zero epoch  $HJD_0 = 2455919.67$  corresponds to the first spectrum, and the rotation period of the star is from Kóvári et al. (2004). Times are given relative to  $HJD_0$ . The color table of the figure was prepared to represent the basal emission with blue-green colors and the sporadic flares with orange-red colors. The basic criterion that we used is that the EW of the  $H\alpha$  flare contribution should be clearly larger than the EW of the neighboring basal contribution. A clear and unambiguous distinction between the two sources was nevertheless not always possible. To prevent the misclassification of optically-thin material seen off-limb as flares, we also required that the Balmer decrement  $F_{H\alpha}/F_{H\beta}$  should not exceed the neighboring values. However, this approach is maybe too simple to account for some of the  $H\alpha$  lines with EWs near  $1.2 \text{ \AA}$ . In principle, they could correspond, for example, to a slightly higher than usual basal emission due to enhanced microflare or network activity, the early or late stages of a more powerful flare, or an intense event but with small projected area. This makes difficult to be sure about the exact amount of flares detected, but using EWs of  $1.2 \text{ \AA}$  and  $1.15 \text{ \AA}$  as threshold values we believe to have seen between 7 and 12 flare events, respectively. The  $H\beta$  line shows only 7 events whose emission is clearly above the basal contribution (bottom panel of Fig. 1).

It appears that the flare activity was more intense at the beginning of our observing campaign than at later stages. Almost as many flares were detected during the first twenty days as during the following three and a half months. They were also more intense and occurred concentrated between phases 0.4 and 0.7. As a consequence of the fast rotation of the star and the given sampling of the observations, none of the detected flares was observed in its full extension. The total duration of the events is therefore unknown, but in some cases it is longer than five hours. A more detailed description of the flare with the best time coverage and its post-flare phase is presented in Sect. 3.3.

### 3.2. Basal emission

It is well known that LQ Hya exhibits cool spots that correlate well with the chromospheric emission (Strassmeier et al. 1993; Frasca et al. 2008; Cao & Gu 2014; Paper I). In Paper I we found that the hemisphere of the star centered at phase 0.6 had during our observations a higher concentration of spots and enhanced chromospheric activity than the other side of the star. The difference in the basal emission of these two hemispheres is evident from Fig. 1, where they appear as a green and as a blue band, respectively. The basal emission of the most active hemisphere remained roughly constant during the four months of observations with  $EW_{H\alpha} \approx 1.0 \text{ \AA}$ . We also see that the active regions seem to be moving toward higher phases, surely because their rotation period is slightly longer than the rotation period that we have used to phase our data.

The less active hemisphere of the star shows, on the other hand, a clear temporal evolution. We detect the lowest level of  $H\alpha$  emission at the beginning of our observation and near phase 0.0. The EW of the subtracted  $H\alpha$  line takes then values of  $\approx 0.7 \text{ \AA}$ , which is still a relatively high level of activity. LQ Hya  $H\alpha$  lines with this emission have their core almost at the continuum level (see Fig. 2. in Paper I). The chromospheric activity from that hemisphere undergoes then a slow but constant rise in its

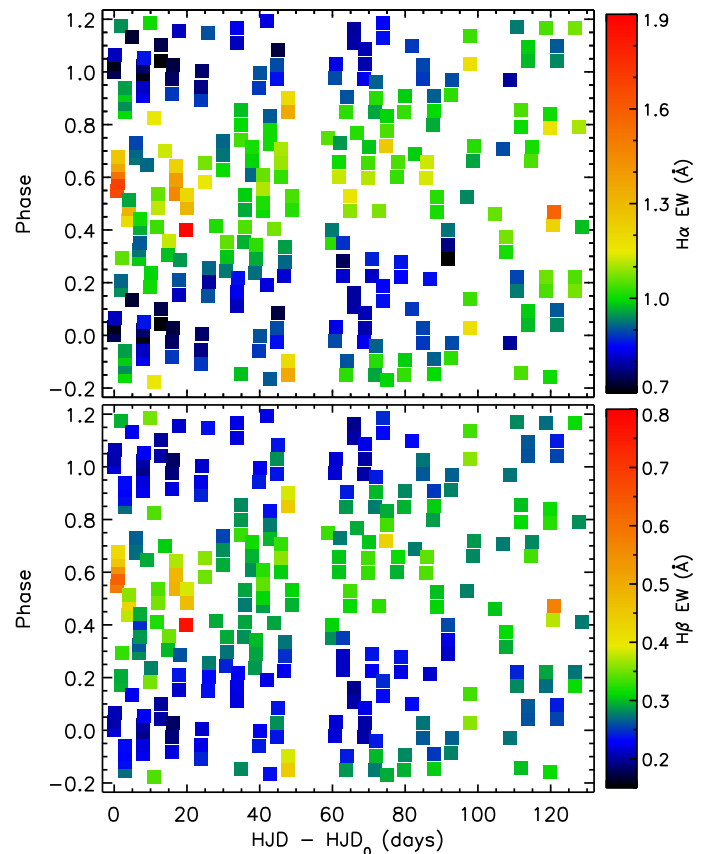


**Figure 1.** Temporal evolution of the equivalent width of the  $H\alpha$  and  $H\beta$  emission profiles (top and bottom panels, respectively) at different rotational phases. Blue-green points correspond to measurements of the basal emission. Orange-red values correspond to sporadic flares.

emission. The  $H\alpha$  equivalent width takes values of  $\approx 0.8 \text{ \AA}$  at the middle of the observations, and between  $0.9$  and  $1.1 \text{ \AA}$  during the last two weeks, meaning that the less active side of the star reached at the end of the observations values that until then had been detected only on the opposite hemisphere. Nonetheless, its average  $H\alpha$  emission was still slightly below that of the opposite side. The  $H\beta$  line, on the other hand, shows a more pronounced rotational modulation when the observations finished.

### 3.3. $H\alpha$ line asymmetries: possible mass ejection

As the original purpose of our observations was the study of the photospheric spot evolution on a time scale of several months, rather than the analysis of flares, the cadence and integration time with which our spectra were collected are generally not optimal for a detailed study of flare evolution. The exception to this was the long duration flare detected the second day of observations (2011 December 25) and the associated post-flare activity observed during the two following days. To study the variations of the line profiles and their asymmetries, we subtracted a quiescent spectrum defined as the average of the spectra with  $F_{H\alpha} \leq 3.5 \times 10^6 \text{ erg cm}^{-2} \text{ s}^{-1}$  ( $EW_{H\alpha} \lesssim 0.8 \text{ \AA}$ ). The reason of taking an average profile as reference is to reduce the noise of the template, and the effect that telluric lines and possible rotational modulations could have on the line asymmetries. The resulting evolution of the profiles can be seen in Fig. 2. In Paper I we evaluated the EW of the net emission profiles after the subtraction of

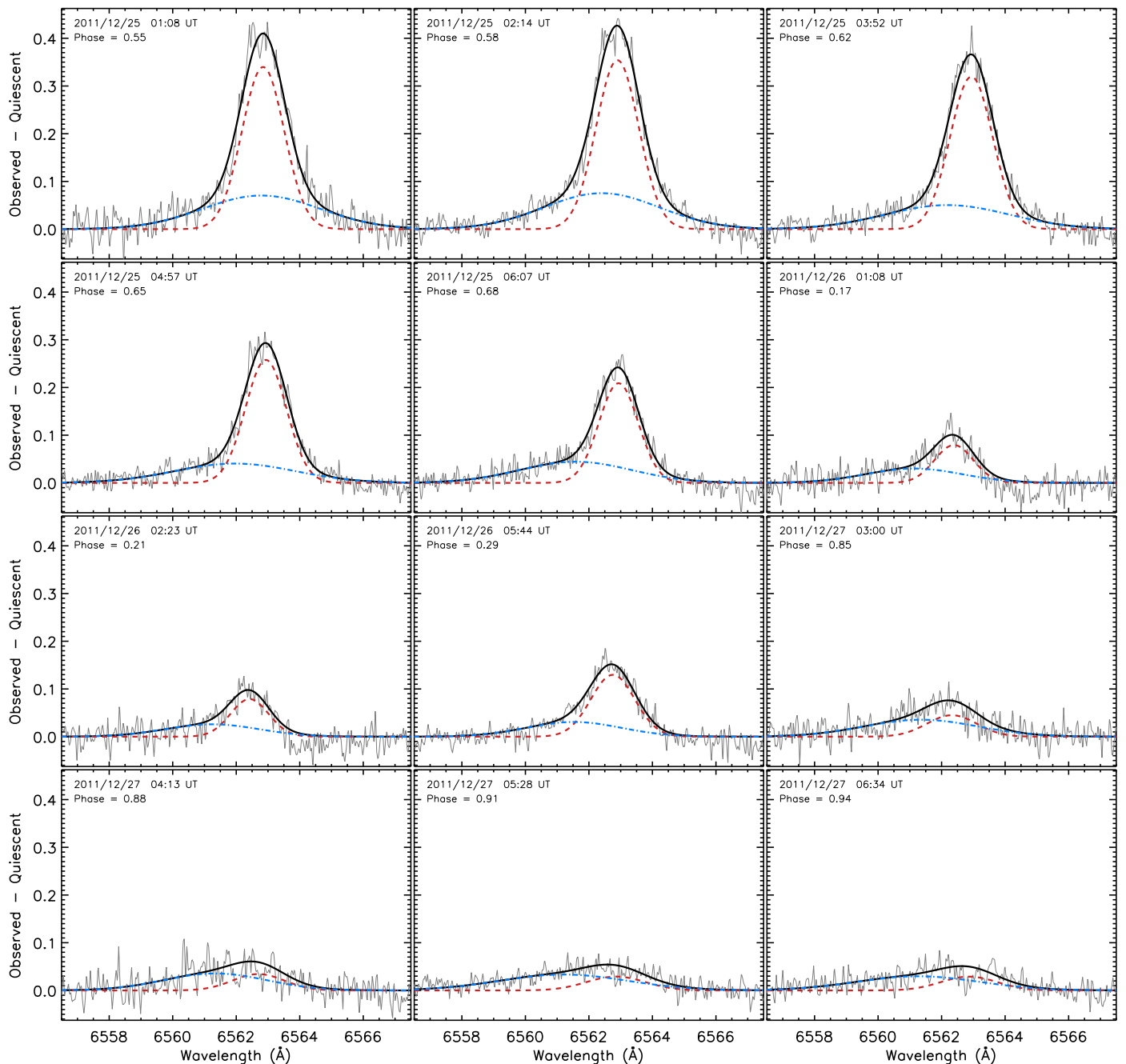


**Figure 2.** Two Gaussian fit (thick solid) of the subtracted  $H\alpha$  profiles (gray solid) of a flare and post-flare spectra. The narrow and broad Gaussian components are depicted as a red dashed, and as a blue dash-dotted line, respectively. Time proceeds from top left to bottom right.

the spectrum of a non-active star. We refrain here from using the same spectrum because it introduces some weak asymmetries in the profiles.

The subtracted profiles show enhanced emission in the wings of the lines. This is a well known effect of flares on Balmer lines, and has already been observed by several authors (see, e.g., Doyle & Byrne 1987; Doyle et al. 1988; Phillips et al. 1988; Eason et al. 1992), also in LQ Hya (Montes et al. 1999). Single-Gaussian fits of these profiles give a poor description of the lines, and a second, broader, and usually shifted Gaussian is necessary for an acceptable fit. To evaluate the parameters of the Gaussians and their uncertainties, we fit each subtracted profile one thousand times with a set of randomly generated initial con-

ditions. The solution for each line is then the weighted mean of all these evaluations, while their uncertainties are the weighted standard deviation. As weighting factor we used the chi-square goodness of the fit. This process is not really necessary when the emission is high because the solution is then well constrained. Nevertheless, when the emission is low the problem becomes ill-posed and many solutions are possible within the uncertainties. The resultant two-Gaussian fit of the profiles, with a broad and a narrow component, is shown in Fig. 2. The numerical values are available in Table 1, where we also indicate the improvement in using two Gaussians rather than one as the ratio of the chi-square goodness of the fits  $\chi_{1G}^2/\chi_{2G}^2$ .

**Table 1.** Parameters of the subtracted H $\alpha$  lines and their broad and narrow Gaussian components during the flare and post-flare.

HJD – HJD <sub>0</sub> (days)	Phase	EW (Å)	$\chi^2_{1G}/\chi^2_{2G}$	Broad component			Narrow component		
				$I \times 10^{-2}$	$\Delta\lambda$ (km s <sup>-1</sup> )	FWHM (Å)	$I \times 10^{-2}$	$\Delta\lambda$ (km s <sup>-1</sup> )	FWHM (Å)
0.88	0.55	1.66 ± 0.02	1.4	7.0 ± 0.3	0 ± 2	4.4 ± 0.1	34.0 ± 0.3	3 ± 1	1.57 ± 0.02
0.92	0.58	1.69 ± 0.01	1.9	7.5 ± 0.3	-18 ± 3	4.3 ± 0.1	35.4 ± 0.4	5 ± 1	1.58 ± 0.02
0.99	0.62	1.53 ± 0.01	1.6	5.0 ± 0.3	-28 ± 6	4.6 ± 0.1	31.9 ± 0.4	7 ± 1	1.58 ± 0.01
1.04	0.65	1.36 ± 0.01	1.6	4.0 ± 0.3	-38 ± 6	4.5 ± 0.1	25.8 ± 0.4	7 ± 1	1.52 ± 0.03
1.09	0.68	1.26 ± 0.01	1.9	4.4 ± 0.2	-55 ± 5	4.2 ± 0.1	20.9 ± 0.3	7 ± 1	1.46 ± 0.02
1.88	0.17	0.94 ± 0.01	1.1	3.0 ± 0.3	-76 ± 9	3.6 ± 0.2	7.9 ± 0.5	-18 ± 3	1.44 ± 0.09
1.93	0.21	0.92 ± 0.01	1.0	2.6 ± 0.3	-71 ± 9	3.5 ± 0.2	7.9 ± 0.4	-17 ± 2	1.42 ± 0.07
2.07	0.29	1.06 ± 0.01	1.1	3.1 ± 0.4	-58 ± 12	3.5 ± 0.3	13.0 ± 0.5	-2 ± 1	1.63 ± 0.04
2.96	0.85	1.00 ± 0.01	1.0	3.5 ± 0.5	-66 ± 10	4.2 ± 0.4	4.5 ± 0.5	-21 ± 9	1.85 ± 0.12
3.01	0.88	0.94 ± 0.02	0.9	3.6 ± 0.4	-67 ± 10	3.8 ± 0.3	3.4 ± 0.5	-4 ± 11	1.91 ± 0.18
3.06	0.91	0.99 ± 0.01	1.0	3.3 ± 0.3	-73 ± 12	4.8 ± 0.4	2.9 ± 0.4	3 ± 11	2.17 ± 0.19
3.10	0.94	0.96 ± 0.01	1.0	3.0 ± 0.3	-70 ± 13	4.6 ± 0.3	2.9 ± 0.4	3 ± 13	2.08 ± 0.22

**Notes.** Times are relative to HJD<sub>0</sub> = 2455919.67. The equivalent widths are from Paper I and were evaluated after the subtraction of a non-active template. The line shifts  $\Delta\lambda$  are relative to  $\lambda_{H\alpha} = 6562.79$  Å.

The spectroscopic observations of the flare consist of five spectra collected with a cadence somewhat higher than one hour. All of them were taken near rotational phase 0.6, with the active hemisphere of the star in its best view. The highest H $\alpha$  emission is detected in the second spectrum of the night. The H $\alpha$  EW of the first spectrum is just 0.03 Å below the maximum, and could correspond to the very end of the impulsive phase. The remaining three spectra show the slow decay of the flare. When the observations finished that night, the EW was 1.26 Å, still 26% above the basal emission. The broad component of the subtracted H $\alpha$  profile also shows clear variations. The first spectrum has its both Gaussians practically aligned at  $\lambda_{H\alpha} = 6562.79$  Å, but afterwards the broad component moves toward shorter wavelengths. The last spectrum of the flare shows the broad Gaussian blue-shifted by  $\approx 1.2$  Å (55 km s<sup>-1</sup>) relative to  $\lambda_{H\alpha}$ .

Although the flare was not observed in its full extension, a lower limit of the energy released in the H $\alpha$  and H $\beta$  lines can be estimated by converting the radiative fluxes from Paper I into luminosities and integrating them over time. To isolate the contribution of the flare from the basal emission we assumed  $F_{H\alpha} = 4.3 \times 10^6$  erg cm<sup>-2</sup> s<sup>-1</sup> and  $F_{H\beta} = 1.6 \times 10^6$  erg cm<sup>-2</sup> s<sup>-1</sup> as the amount of flux received from the undisturbed chromosphere. This leads to the energies  $E_{H\alpha} > 5.2 \times 10^{32}$  erg and  $E_{H\beta} > 3.1 \times 10^{32}$  erg if a radius  $R_{\text{star}} = 0.97 R_{\odot}$  is adopted (Kővári et al. 2004). In comparison, Montes et al. (1999) measured  $E_{H\alpha} > 2.5 \times 10^{33}$  erg and  $E_{H\beta} > 2.1 \times 10^{33}$  erg for a different LQ Hya flare.

One day after the flare the star was observed near rotational phase 0.2. This corresponds mostly to the most quiet hemisphere of the star, but with the active hemisphere already visible near the limb. At that time the EW of the H $\alpha$  line was near 0.9 Å, which is within the usual range of values for the basal emission at that phase. But even though the H $\alpha$  emission is comparably low, the line shape had a blue wing with excess emission. The broad Gaussian component of these profiles is weaker than in the spectra taken the day before and also slightly more blue-shifted than in the last flare spectrum. Considering that we did not observe this kind of behavior in any other spectra from the same phase, we speculate that it could be related to the flare observed

the day before. The last spectrum of the night was taken at phase 0.3 and shows a small increment in the emission. It is likely because of the increment of the projected area of the active regions appearing from the limb, but could have been also due to a minor flare.

Two days after the strong flare the blue wing of the H $\alpha$  line still presents excess emission. Four spectra taken near phase 0.9 are available from that night. The emission from the core was then clearly lower than the day before, but the emission of both wings was slightly enhanced. This could be a physical process or maybe a somewhat misplaced continuum. A single-Gaussian fit of the subtracted profiles provides here an acceptable result. Nevertheless, to look for a continuity in the behavior of the broad component, we forced our code to use two Gaussians, one of them as a narrow component with center near  $\lambda_{H\alpha}$ . By doing so, we find broad components that are wider than the day before but placed at the same position. The time evolution of the line shifts in velocity scale is shown in the top panel of Fig. 3.

The asymmetries of the Balmer lines are usually interpreted as a consequence of plasma turbulence or directed mass motions. Houdebine et al. (1990) found a large enhancement in the far blue wings of Balmer lines during the impulsive phase of a flare on AD Leo, that they attribute to a mass ejection. Houdebine et al. (1993) found in the same flare red-shifted Balmer line cores that were interpreted as a chromospheric downward condensation. Blue-shifted asymmetries in the Balmer lines of AT Mic were interpreted by Gunn et al. (1994) as a result of a high-velocity chromospheric evaporation during a flare. Montes et al. (1999) performed a multi-line analysis of an unusually strong flare on LQ Hya and detected asymmetric profiles that were blue-shifted during the impulsive phase and red-shifted during the gradual decay. They attribute the broad components and the asymmetries to plasma turbulence or to upward and downward mass motions.

Although the measurements are too sparse in time to conclude beyond all doubt that the excess emission in the blue wing of the H $\alpha$  line is the consequence of a single event, we speculate that the source could be some kind of material ejected during the flare. The excess emission was detected in the H $\alpha$  line but

**Table 2.** Time interval covered by each Doppler map.

Group	Time range		Days	Spectra	Spectra per map	Photom. points
	HJD – HJD <sub>0</sub>	Date				
1	0 - 21	2011/12/24 - 2012/01/15	22	56	29	34
2	22 - 53	2012/01/15 - 2012/02/16	32	55	47	57
3	54 - 80	2012/02/16 - 2012/03/14	27	41	30	626
4	81 - 102	2012/03/14 - 2012/04/05	22	22	19	179
5	103 - 129 (+11)	2012/04/05 - 2012/04/30 (+11 d)	27 (+11)	25	13	248

**Notes.** To facilitate the comparison, we divided the photometry from Fig. 4 in the same five groups. The last group covers for the photometry eleven additional days for which we do not have spectroscopic data. HJD<sub>0</sub> is the same as in Tab. 1.

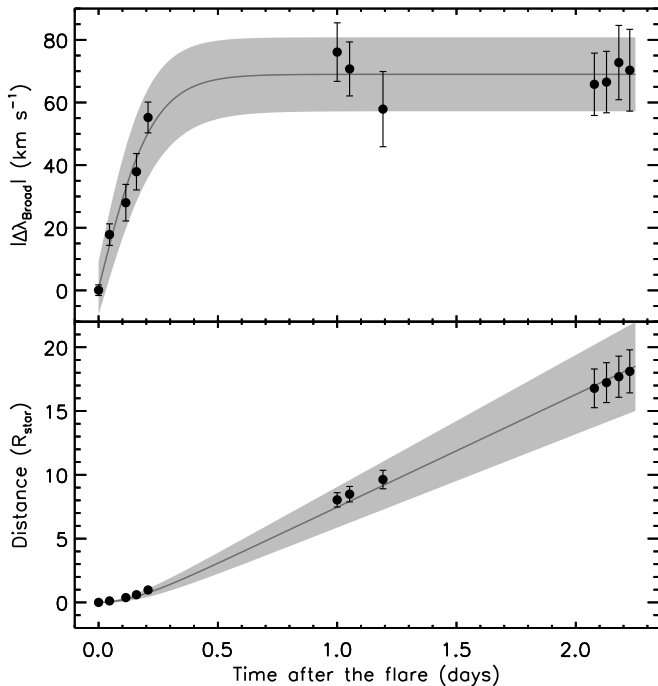


**Figure 3.** *Top:* absolute shift of the broad Gaussian component of the H $\alpha$  line from Fig. 2, in velocity scale. The data have been fit to Eq. (1) (solid line). The gray area indicates the 95% confidence intervals of the fit. *Bottom:* distance traveled by the source of the broad component under the assumption that it corresponds to ejected material. Data points are from the numerical integration of the velocity measurements. The solid line is the integral of the function used to fit the velocities.

not in H $\beta$ , which could indicate that the emission came from optically thin material seen off-limb. Additionally, it was observed at different rotational phases, for as long as two days after the flare, and always blue-shifted. This lack of rotational modulation could suggest that the source of emission is not attached to the stellar surface and that it is not corotating with it. Furthermore, the velocity profile calculated from the line shifts (top panel of Fig. 3) is remarkably similar to that of many solar coronal mass ejections (see, e.g., Gallagher et al. 2003; Bein et al. 2011).

Under the hypothesis of the mass ejection, we estimated the distance that the material could have traveled. We first fit the velocities to a function of the form

$$v(t) = \frac{a}{e^{-bt} + 1} - c, \quad (1)$$

where  $t$  is time, and  $a$ ,  $b$  and  $c$  are the fitting parameters. The function was chosen because it reproduces well the behavior of the data, with a fast and short acceleration phase, and a long asymptotic phase of constant velocity. The gray areas of Fig. 3 are the 95% confidence intervals of the fit. Once the fitting function was evaluated, we determined the distances by just integrating it (lower panel of Fig. 3). According to this, the distance traveled would be of  $\approx 18 R_{\text{star}}$ , where we took  $R_{\text{star}} = 0.97 R_{\odot}$  from Kóvári et al. (2004). We note that because of the use of projected velocities, this distance is only a lower limit.

We conclude this section with a brief summary about the H $\alpha$  line asymmetries in the rest of the spectra. The two Gaussian fits of the H $\alpha$  lines with  $EW \lesssim 1.0 \text{ \AA}$  do not show any improvement over the use of a single Gaussian. On the other hand, the use of two Gaussians improves the fit of all H $\alpha$  lines with  $EW \gtrsim 1.1 \text{ \AA}$  by at least 10% in terms of the chi-square goodness of the fit. When the EW is in the range 1.0-1.1  $\text{\AA}$  roughly half of the fits show some improvement if two Gaussians are used. We note, however, that these values depend on the selection of the “quiescent” spectrum. Approximately 40 spectra show H $\alpha$  lines with a shifted broad component, most of them red-shifted.

Montes et al. (1998) analyzed the H $\alpha$  line in chromospherically active binary systems and in weak-lined T Tauri stars. They detected in the most active stars of the sample broad wings that in some cases were also asymmetric. By similarity with the behavior of transition region lines, they interpreted this excess emission as arising from microflare activity. We have found a comparable behavior in the lines from the most active hemisphere of LQ Hya. This suggest that at least part of the basal emission from that side of the star could be produced by low intensity flares occurring on a regular basis, supporting our results from Paper I. A few examples of these lines are shown in the appendix in Fig. A.1.

## 4. Evolution of the photospheric spots

### 4.1. Photometric light curves

To facilitate the comparison between the photometric light curve and the Doppler maps of Sect. 4.2, we have divided them into the same five time intervals (Tab. 2). The photometry of the last group covers eleven additional days for which we do not have any spectral data. Data collected during the first 58 days of observation (first and second groups) are affected by larger error bars. Nevertheless, we include the best measurements for completeness and because they could still provide some guidelines about the evolution. More than a half of the photometric data were taken during the time span covered by the third group. This high number of measurements together with their significantly

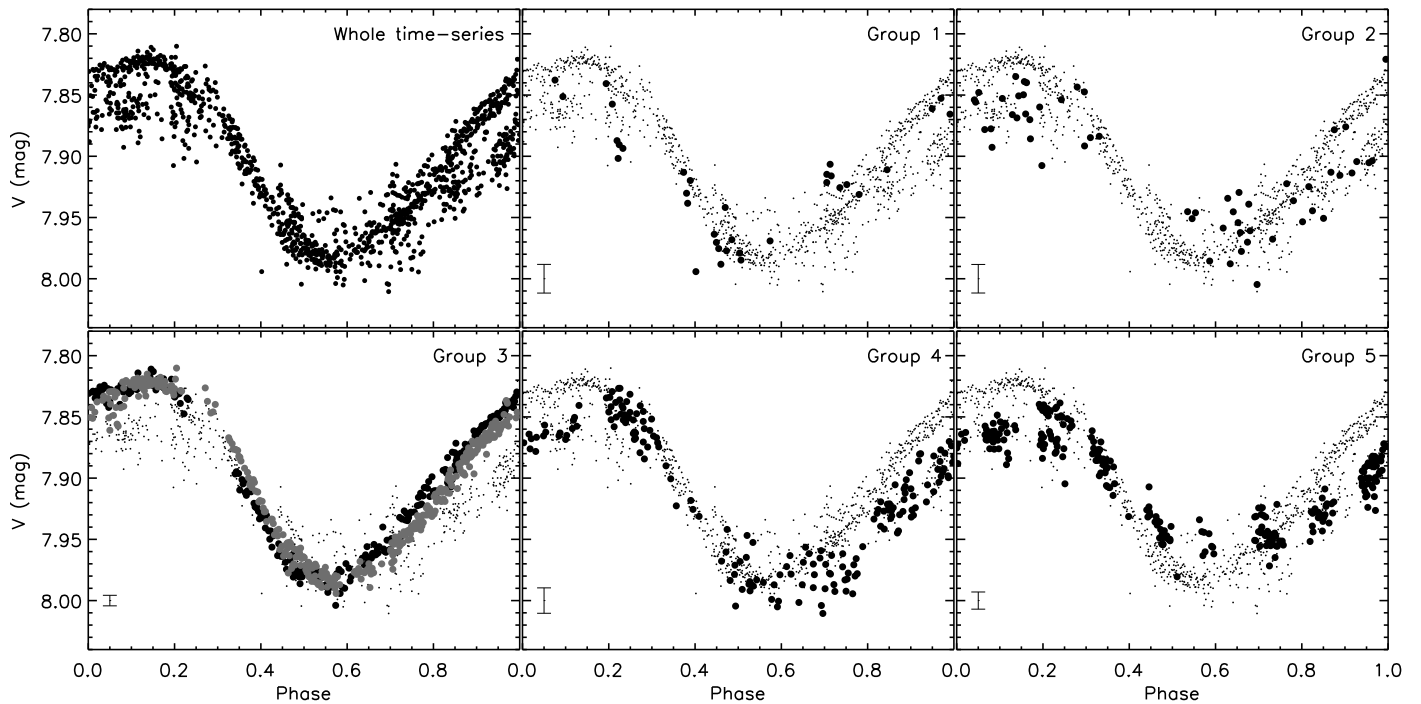


**Figure 4.** Rotational modulation of the  $V$ -band photometry at different time intervals. *Top left:* for the whole time-series. *Top middle:* for days 0 to 21. *Top right:* for days 22 to 53. *Bottom left:* for days 54 to 66 (black circles) and for days 67 to 80 (gray circles). *Bottom middle:* for days 81 to 102. *Bottom right:* for days 103 to 140. Average error bars for each group are given in the lower left corner of each panel. Small dots correspond to the measurements of the whole time-series and are included as a reference to facilitate the comparison. Times in calendar dates are available in Table 2.

smaller error bars, make possible to see the evolution at a shorter time scale. For these reasons we have divided this group into two subgroups.

The top left panel of Fig. 4 shows the phase-plot of the whole time-series. As reported in Paper I, the photometry shows clear rotational modulation, indicating a higher concentration of dark spots on one side of the star. Although this configuration is relatively stable in time, it is still possible to see some evolution. In the third group (bottom left panel of Fig. 4) we observe that the time of minimum brightness moves toward higher phases. As for the chromospheric emission, this can be easily explained if the rotation period of the spots were slightly longer than the  $P = 1.60066$  d period used to phase the data. Nevertheless, subsequent data show that this can not be the only reason. We see that while the hemisphere of minimum brightness moves from phase  $\sim 0.5$  to phase  $\sim 0.6$ , the peak-to-peak variation of the light curve decreases from  $0^m16$  in the third group to  $0^m09$  at the end of the observations. Contrary to what we observe for the basal  $H\alpha$  emission, the  $V$  brightness of the less active side of the star takes always values that are clearly different from those of the opposite hemisphere. We also note that the changes in the light curve take place while the mean brightness of the star remains roughly constant at a value of  $V \approx 7.90$  mag. This indicates that the main reason of variability could be the redistribution of spots on the stellar surface, rather than the emerging of new or decay of old active regions. Finally, the unspotted magnitude of LQ Hya is thought to be near  $V = 7.76$  mag (see, e.g., Strassmeier et al. 1993), which is clearly brighter than our maximum value of  $V = 7.82$  mag. This suggests that not even the most quiet hemisphere of LQ Hya was completely spotless during our observations.

## 4.2. Doppler imaging

### 4.2.1. Line inversion

The chromospheric  $H\alpha$  emission and the photometric light curve clearly indicate that the surface activity of LQ Hya was changing over time. As they alone can not show the ultimate cause of the changes, we have spatially resolved the surface of the star by means of Doppler imaging. We inverted the line profiles with the algorithm developed by Constable et al. (1987) and deGroot-Hedlin & Constable (1990). The local line profiles were computed with the program SPECTRUM (Gray & Corbally 1994) for a grid of  $60 \times 30$  surface elements. We used the model atmospheres from Kurucz (1993), the stellar parameters from Kővári et al. (2004), and the chemical abundances from Rice & Strassmeier (1998) (Table 3). The result of the inversions are shown in Fig. 5.

Particularly problematic for the inversion was the rather high level of noise in the spectra. The spots of LQ Hya have only a relatively weak effect on the line profiles (see Fig. B.1 in the appendix), and an average S/N of 74 is certainly far lower than ideal for Doppler imaging. To minimize this problem, we inverted simultaneously 19 line profiles (Table 4), whose level of noise was previously reduced with the PCA denoising procedure described by Martínez González et al. (2008). Neighbor lines affecting those profiles were also taken into account for the inversion. In addition to the noise, magnetic activity phenomena other than photospheric spots also seem to be affecting the shape of the spectral lines. We noted that several line profiles are different to others taken at a similar phase and time. This is particularly evident at the beginning of the observations, when the flare activity was more intense. Typical effects are the line filling produced during flares, and line asymmetries that could be attributed to the

**Table 3.** Parameters of LQ Hya adopted for the inversion of the line profiles.

Parameter	Value
Spectral type	K2 V
$\log g$	4.0
$v \sin i$	28.0 km s <sup>-1</sup>
Inclination, $i$	65°
Rotation period, $P_{\text{rot}}$	1.60066 d
Radius, $R$	0.97
Microturbulence	0.5 km s <sup>-1</sup>
Macroturbulence	1.5 km s <sup>-1</sup>
Fe abundance	solar + 0.1 dex
Ca abundance	solar + 0.1 dex
Ni abundance	solar + 0.3 dex
Abund. other elements	solar

**Notes.** The physical parameters are from Kóvári et al. (2004) and the chemical abundances from Rice & Strassmeier (1998).

**Table 4.** Spectral lines used for the inversion, together with the adopted  $\log gf$  and energy of the lower state.

Element-Ion	$\lambda_{\text{cent}}$ (Å)	$\log gf$	$E_{\text{low}}$ (cm <sup>-1</sup> )
Fe I	5429.696	-1.879	7728
Fe I	5501.464	-2.957	7728
Fe I	5569.618	-0.633	27560
Fe I	5572.841	-0.311	27395
Fe I	5576.090	-1.01	27666
Ca I	5581.965	-0.510	20349
Ca I	5594.462	0.15	20349
Ca I	5598.480	0.034	20335
Ca I	5857.451	0.257	23652
Fe I	5914.194	-0.059	37163
Fe I	6024.049	0.091	36686
Fe I	6191.558	-1.377	19621
Fe I	6400.009	-0.290	29056
Fe I	6411.658	-0.718	29469
Fe I	6430.856	-2.006	17550
Ca I	6439.081	0.470	20371
Ca I	6462.570	0.30	20349
Ca I	6717.688	-0.24	21850
Ca I	7148.150	0.208	21850

transfer of momentum to the photosphere by down-flows similar to those observed in the Sun (see, e.g., Kosovichev & Zharkova 1998; Venkatakrishnan et al. 2008). Nevertheless, in most cases it is not possible to find the ultimate cause of the discrepancies, as noise itself can have a similar effect. Line profiles affected by these problems were not used in the inversion.

An indirect way to reduce the effect of noise and activity is to use a high amount of spectra per map. To avoid inconsistencies introduced by the natural evolution of active regions, this has to be done using data that cover sufficiently short time intervals. For the computation of the maps we divided the spectra in the five groups indicated in Table 2. With this distribution of spectra we try to have always a good phase coverage, while keeping all groups with a similar length. Nonetheless, this was not always possible because of the nonuniform sampling of our data, and the presence of gaps. We note that the quality of the last map is comparably lower than for the others as a consequence of the poor phase coverage near phase 0.5. Furthermore, the few spec-

tra available from that phase are either affected by a flare or by a low signal to noise ratio.

As an example, we show in the appendix in Fig. C.1 a map computed in the same way as the first map of the time series (top panel of Fig. 5) but including some spectra that were rejected for the final solution. These spectra are those in which the H $\alpha$  line seems to be affected by a mass ejection (see Sect. 3.3), but that are undisturbed by the flare that could have produced it (i.e., the last seven spectra of Table 1). In this version of the map the near equatorial spot is no longer present, the temperature of the bridge between the two high latitude spots decreases  $\approx$  120 K to values near those from their cores, and a new spot appears near phase 0.85. Nonetheless, our data suggest that this new spot is not a real cool spot. It appears on the least active side of the star at a time when the chromospheric emission had its lowest values, it does not seem to have any effect on the photometry, and it is not observed in spectra that were taken just three days after and three days before than the rejected spectra nor in any other map. It can also be noted that after removing the affected spectra a 0.2 phases wide gap appears near phase 0.85. This gap is nonetheless not big enough to explain the absence of the spot. Because of its high latitude, if the spot were real it should have been detected by means of the spectra taken within a window of  $\pm 0.25$  phases. Although the distortions in the spectral lines that produce the discrepancies between the two maps are maybe not a consequence of the ejected material itself, this result suggests that flare activity could affect the results of line inversions even when the flare emission has already vanished. We note that the source of these differences could be also affecting the final version, although in a much slighter degree. It shows a very weak spot at phase 0.85 and the near equatorial spot is fainter than in the other maps.

#### 4.2.2. Doppler maps

Figure 5 reveals that three spots dominated the surface activity of LQ Hya during the period of time covered by our observations. They are a low-latitude spot (S1), and two spots at higher latitudes (in Fig. 5, from left to right, S2 and S3). This spot configuration remained stable and indicates that active regions on LQ Hya can easily live for periods of time longer than four months, with little or no signs of evolution other than changes in their position. Although some maps also show fluctuation of the spot's temperature by up to  $\approx$  200 K, this could be attributed to the limited S/N of the data and to flare-related events. For example, the higher temperature of S3 in the third map seems to be a consequence of inconsistencies in some line profiles that also lead to a morphological distortion, and the increment in the temperature of S2 in the fifth map is likely produced by the poor coverage near phase 0.5. The difference in temperature between the quiet photosphere and the spots does not exceed here 500 K, in good agreement with the results of Strassmeier et al. (1993) and Rice & Strassmeier (1998). In the maps the temperature of the quiet photosphere is near 4900 K. This is  $\approx$  100 K lower than the maximum hemispheric temperature that we found in Paper I, which is not a dramatic difference if we consider that the inversion has not been optimized for the accurate determination of stellar parameters other than the position of the spots.



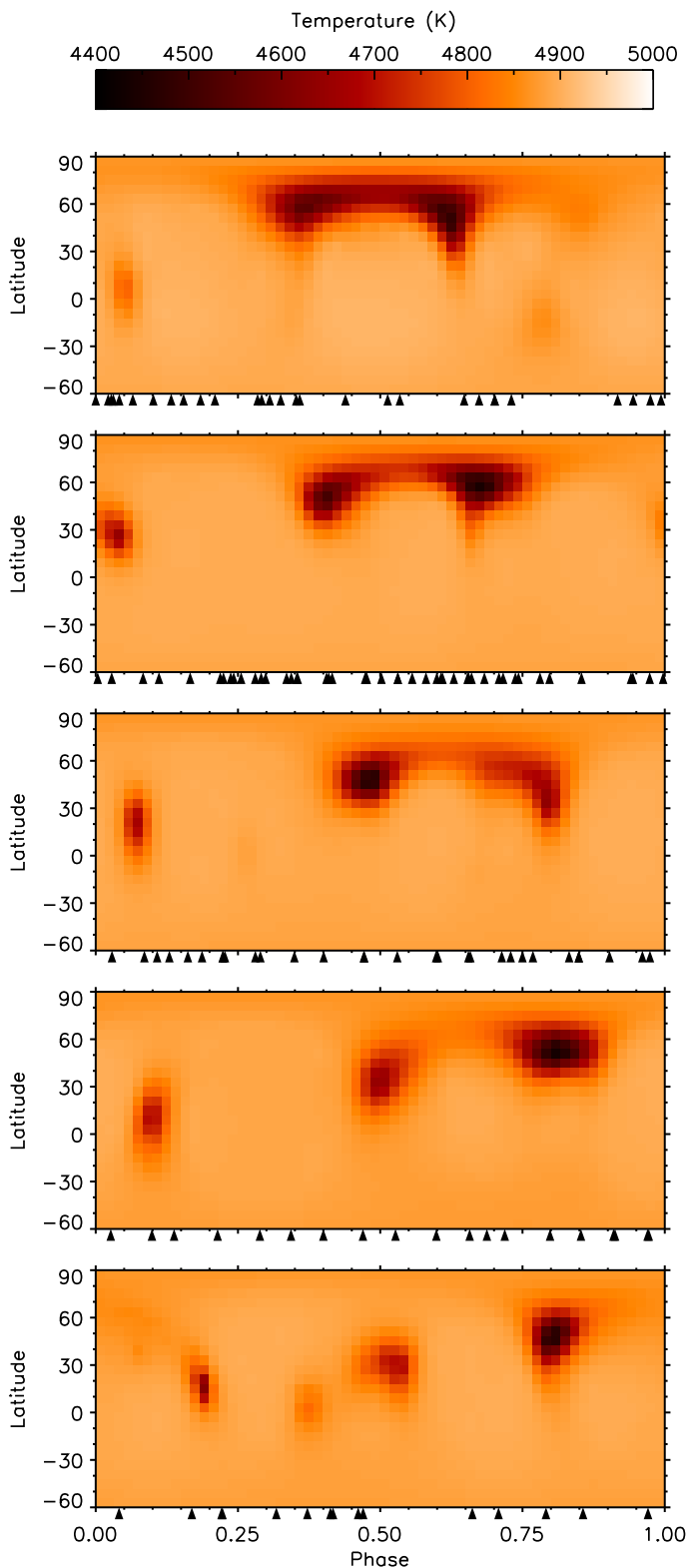


**Figure 5.** Time series of Doppler maps for the period December 2011 - April 2012. Chronological order from top to bottom. Time intervals covered by each map are given in Table 2. Arrows at the bottom of each panel indicate the phase coverage. Spots are dubbed S1, S2, and S3 from left to right in the top panel.

In our maps, all spots show a consistent migration toward higher phases. Furthermore, we note that this migration is faster at high latitudes as compared to lower latitudes, as one would ex-

pect from a star with a solar-like differential rotation. From the first map to the fourth (positions in the fifth map are more uncertain), the low-latitude spot S1 moves 0.05 phases, S2 moves 0.15 phases, and S3 moves 0.20 phases. The fact that the spots cover a high range of latitudes, and that all of them move toward higher phases, indicates that the  $P = 1.60066$  d period used to phase the maps could be slightly underestimated.

Curiously, the latitude of S2 seems to decrease from one map to the next. From the position of the spot center, and the mid time of each map, we derive a velocity of  $\approx 0.26$  deg d $^{-1}$ . If we consider the expected radius of a K2 dwarf  $R = 0.75 R_{\odot}$  (e.g., Gray 2008) and the value  $R = 0.97 R_{\odot}$  found by Kóvári et al. (2004) for LQ Hya, this leads to a meridional speed of 27 m s $^{-1}$  and 35 m s $^{-1}$ , respectively. In comparison, the meridional motion of sunspot groups rarely exceeds 0.1 deg d $^{-1}$  (see, e.g., Wöhl & Brajša 2001). Nevertheless, we note that the determination of latitudes from Doppler imaging is more uncertain than the determination of rotational phases. Some fluctuations are therefore normal. This is observed for the spots S1 and S3, as they irregularly change their latitude by up to 15 deg. The behavior of S2 is, on the other hand, somewhat different, as its latitude decreases monotonically a total of  $\approx 30$  deg. A more detailed analysis of the migration of the spots, including the differential rotation, is deferred to a future and dedicated paper.

The comparison between the Doppler maps and the photometric light curve reveals that the phase of minimum brightness corresponds to the midpoint between the spots S2 and S3. We observe that the motion of the minimum follows the migration of the two spots toward higher phases, and that the amplitude of the light curve decreases as the distance between the spots increases. The darkest side of the star becomes brighter as S2 and S3 separate from each other, while the hemisphere centered at phase 0.1 becomes darker as S3 appears from the limb. S1 seems to play only a minor role in the modulation of the light curve, surely because of its somewhat higher temperature and smaller surface. Nevertheless, it explains why we did not observe the unspotted magnitude of  $V \approx 7.76$  mag, as at least one of the three spots is always on view. This interpretation based purely on the motion of the spots also explains why the average stellar magnitude remains constant.

## 5. Putting things together: connection between spots, plages, and flares

A way to assess the degree of spatial association between photospheric and chromospheric active regions is by cross-correlating the photometric light curve with the phase-resolved estimations of  $EW_{H\alpha}$  and  $EW_{H\beta}$  excluding flares. As this analysis requires a very dense phase-coverage, the results from the first and second groups of Table 2 were combined to increase the amount of photometric data-points, and the results from the last two groups to increase the amount of chromospheric measurements. Each one of the three sets was fit to a high-degree polynomial and then cross-correlated. The result from the first set shows a lag of  $-0.05$  phases, where the negative value indicates that the photometry is ahead in phase. Although this is not a negligible difference and is observed for both  $H\alpha$  and  $H\beta$ , it could be probably just a consequence of the lower quality of the photometric measurements during that period of time. The cross-correlation of the two other data sets shows, on the other hand, differences between  $-0.01$  and  $0.02$  phases, indicating a good match and no clear trend in the lag either for  $H\alpha$  or  $H\beta$ . In comparison, the cross-correlation between the chromospheric data from the first and last sets gives a difference of 0.10 phases.

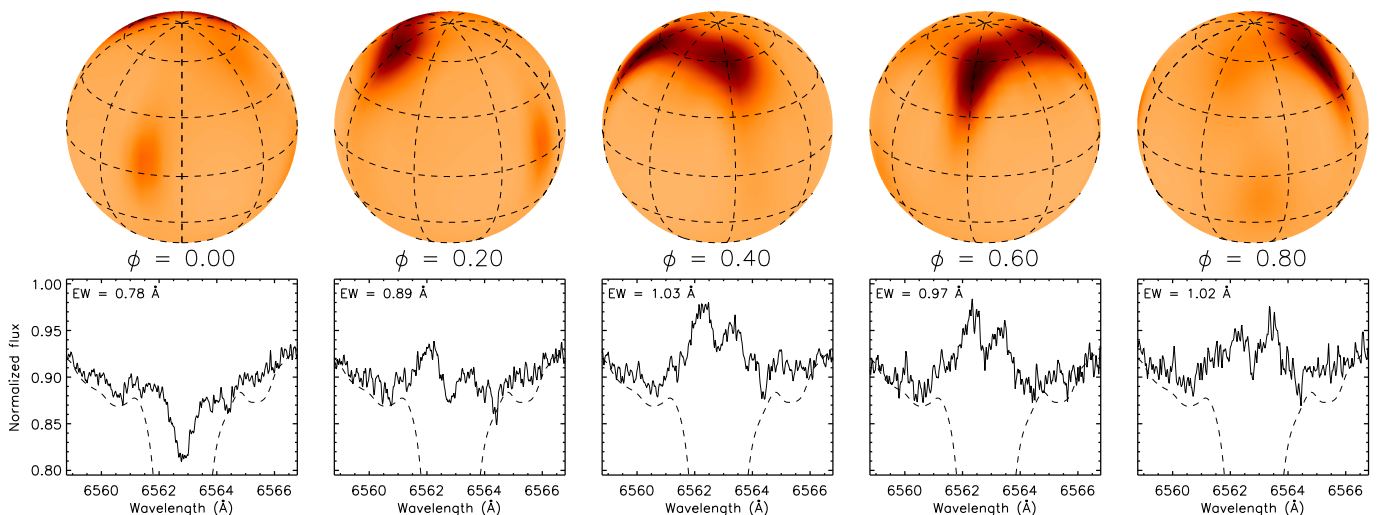


**Figure 6.** Orthographic projection of the first map (data group 1 in Table 2) at five different rotational phases together with the average  $H\alpha$  line at each phase. The spectrum of the non-active reference star HD 3765 is shown as a dashed line. The color table is the same as in Fig. 5.

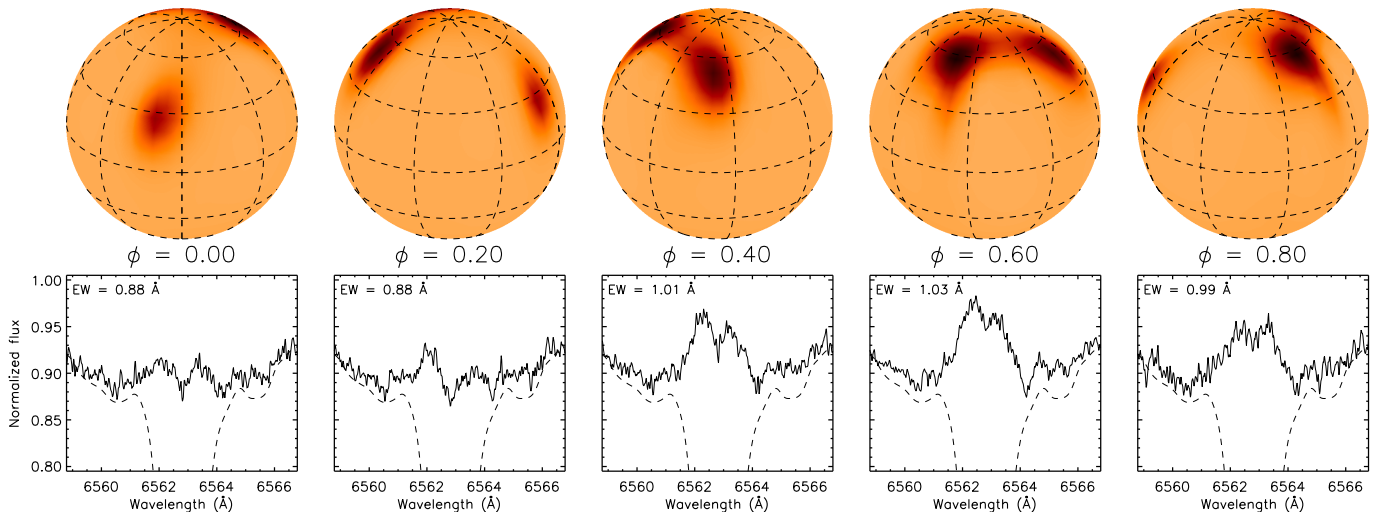


**Figure 7.** Same as Fig. 6 but for the second map (data group 2 in Table 2).

To study in more detail the evolution of the chromospheric activity and its relation with the spots, we computed for each Doppler map the average  $H\alpha$  line at five equidistant rotational phases (0.0, 0.2, 0.4, 0.6 and 0.8). Each average line was calculated using all spectra within a window of  $\pm 0.1$  phases with equal weight.  $H\alpha$  lines with  $EW \geq 1.2 \text{ \AA}$  and those affected by the possible mass ejection were discarded. The resultant average  $H\alpha$  lines are plotted along with the projected stellar hemispheres in Figures 6 to 10.

We observe that the hemisphere centered around phase 0.0 increases its average  $EW_{H\alpha}$  emission by up to  $\approx 0.2 \text{ \AA}$  as the spot S3 becomes visible at the receding side of the star. The hemisphere centered at phase 0.2 corresponds to the region between S1 and S2. Its average  $H\alpha$  line shows a weak decay as S2 becomes less visible (Fig. 6 to Fig. 8), but increases again by almost  $0.1 \text{ \AA}$  when S1 reaches the central meridian. We note that although the first map at phase 0.0 and the last map at phase 0.2 are both centered near S1, their respective  $H\alpha$  lines are significantly different, indicating that the chromosphere above S1 became more active. The emission of the hemisphere centered at phase 0.4 decays as S2 and S3 become less visible, but recovers

its strength when S1 appears. The  $EW_{H\alpha}$  at phase 0.6 increases by  $0.1 \text{ \AA}$  from the first to the third map, when the view is centered at S3 as well as at the midpoint between S2 and S3. No significant  $H\alpha$  variations are observed around phase 0.8, although the line in the first map could have been affected by a minor flare.

This analysis indicates good agreement between the spot locations in the photospheric maps and the variations of the chromospheric  $H\alpha$  line, but also that at least the chromospheric emission associated with the spot S1 evolved significantly. To study the evolution of the chromospheric activity of each active region we repeated the same analysis as before but centering the  $H\alpha$  profiles at the phases of the three spots. In addition, we also included in this analysis the region between the spots S2 and S3 to see whether the chromospheric emission changes as they move apart from each other. The result can be seen in Figures 11 to 14. Although the contribution of each active region can not be easily isolated, it confirms that S1 is the only spot with a significant variation in its chromospheric activity. On that side of the star the EW of the average  $H\alpha$  line increases from  $0.76 \text{ \AA}$  to  $1.00 \text{ \AA}$ . Spots S2 and S3, on the other hand, only show fluctuation of

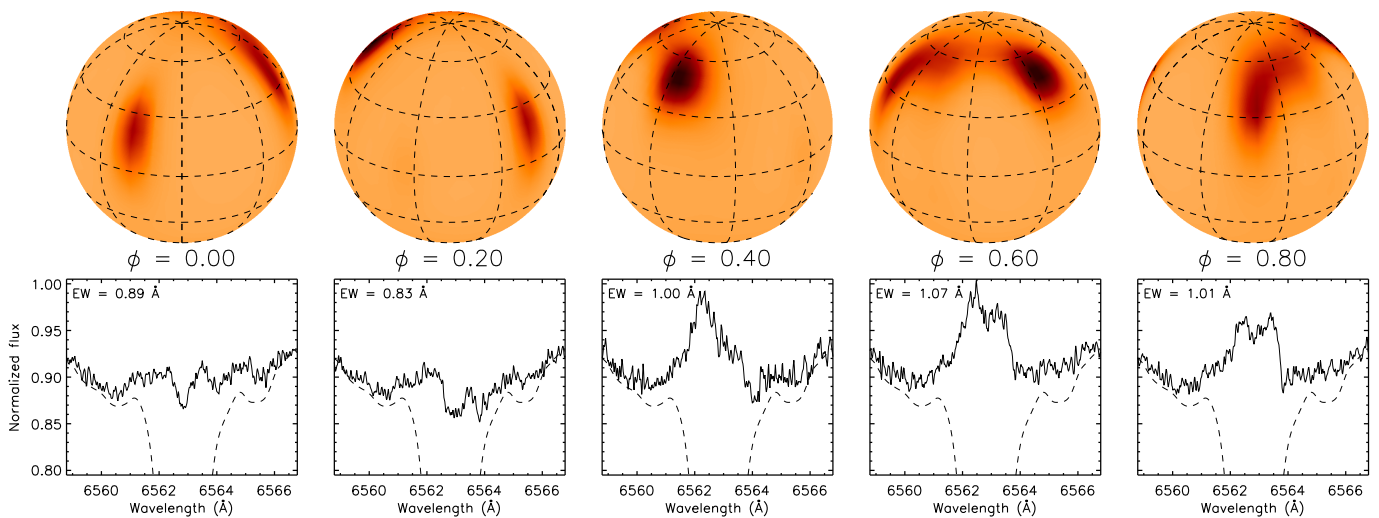


**Figure 8.** Same as Fig. 6 but for the third map (data group 3 in Table 2).

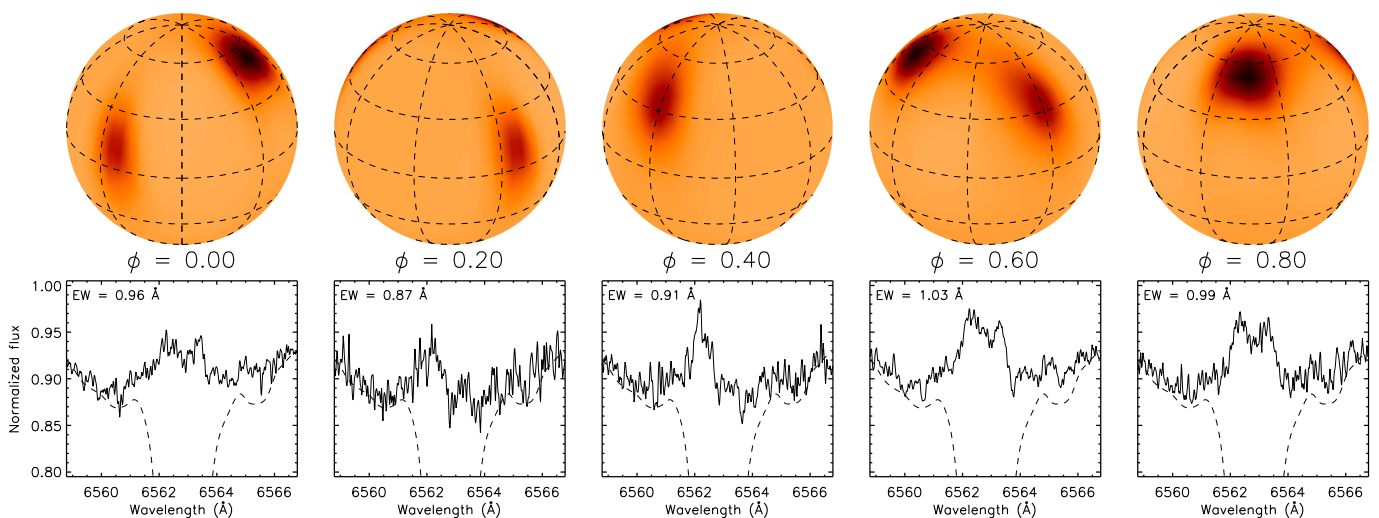


**Figure 9.** Same as Fig. 6 but for the fourth map (data group 4 in Table 2).

0.05 Å. Similarly, the region between S2 and S3 only shows a minor decay in the  $H\alpha$  line of the last map.

The structural changes of the  $H\alpha$  line as the star rotates can also provide some valuable information. The line usually presents a central self reversal and thus two peaks, one on each side of the central wavelength. The two peaks have a similar strength when the active regions are near the meridian. Nevertheless, when one of the spots appears at the limb moving toward the central meridian, the blue peak can be up to a 10% stronger than the other in terms of peak intensity. This effect is particularly evident when the receding side of the star is unspotted (see, e.g., phase 0.2 in Fig. 6 and phase 0.4 in Fig. 9). On the other hand,  $H\alpha$  lines observed when the active region is on the receding side show either two peaks of similar intensity or also the blue peak stronger than the red (see, e.g., phase 0.2 Fig. 9). What we never observed is an asymmetry dominated by the red peak. This indicates that the rotational Doppler shift can be discarded as the sole reason of the line asymmetries.

The region near the red peak of the  $H\alpha$  line is affected by several telluric lines. To test whether the tellurics are the reason why we never observed the  $H\alpha$  profile dominated by a red peak, we simulated their impact in a worst case scenario. Because of the intrinsic variability of the  $H\alpha$  line and the limited S/N,

we isolated the telluric contribution using STELLA spectra of the telluric standard star HD 177724. These spectra were taken when the SES spectrograph was already operating in its nominal resolving power of  $R = 55\,000$ . To enable the direct comparison with the LQ Hya spectra, we reduced the resolution of the HD 177724 spectra to  $R = 30\,000$  with a Gaussian convolution. We then compared both sets of data and chose an HD 177724 spectrum with the telluric water vapor lines slightly stronger than in the most affected LQ Hya spectrum.

The only telluric line that could have a significant impact on the red peak of the  $H\alpha$  line moves monotonically in the LQ Hya spectra from  $\lambda_{\text{ini}} = 6564.5\text{ \AA}$  at the beginning of the observations to  $\lambda_{\text{end}} = 6563.4\text{ \AA}$  at the end. This implies that the telluric line is near the center of the red peak only at the end of the observations. In the data from Figs. 6 to 9 the telluric line is too far away to suppress the red peak. Additionally, we also reversed  $H\alpha$  profiles dominated by a blue peak around the wavelength  $\lambda_{H\alpha} = 6562.79\text{ \AA}$ . In this way, the blue peak appears in the position of the red peak. We used then the telluric template to contaminate those profiles. We see that even in the worst case scenario the telluric line is too sharp compared to the red peak to completely suppress it. An example is shown in the appendix in Fig. D.1. We can therefore conclude that the telluric lines can

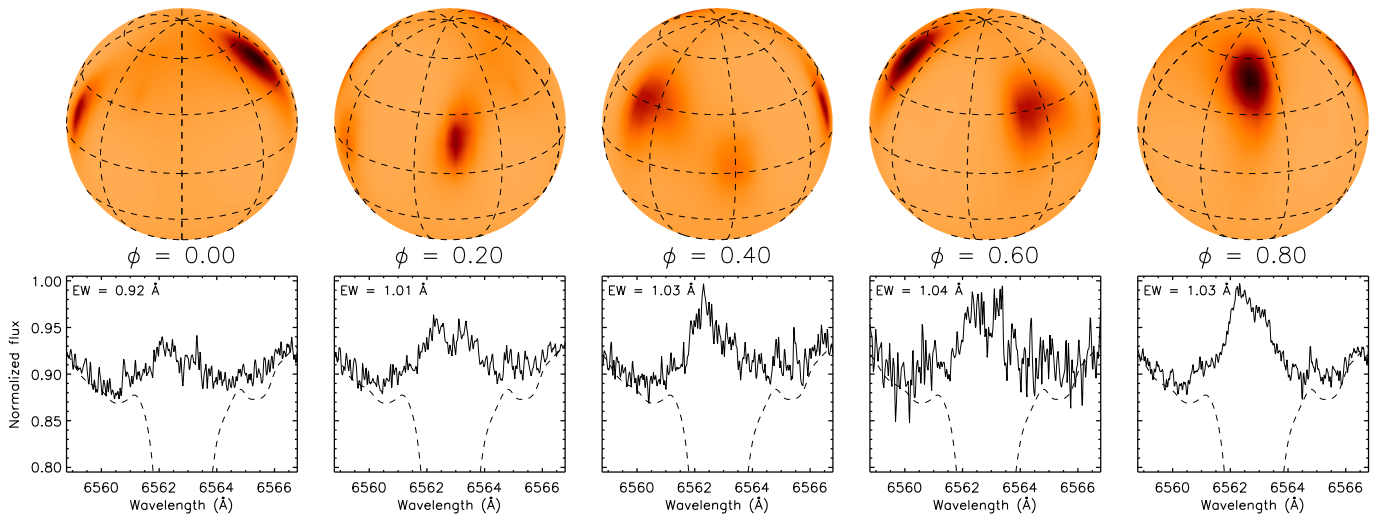


**Figure 10.** Same as Fig. 6 but for the fifth map (data group 5 in Table 2).

explain second order asymmetries but not the fact that some  $H\alpha$  lines have only a blue peak, nor that the red peak never dominates the profile.

Considering that the blue asymmetry is strongest when the spot is on the limb, and that it disappears when the spot is on the meridian, we suggest that the source could be a flow of moving magnetic features surrounding the spots, parallel to the stellar surface, and maybe analogous to the solar Evershed effect or to the moat flow.

More difficult to explain in view of our data is the sharp decay of the sporadic flare activity. These flares were habitual during the first 20 days of observations but then they became more occasional and delocalized from the most active hemisphere. This corresponds to the epoch of closest distance between the spots S2 and S3, suggesting that the flares could have been the result of the interaction between the magnetic fields of these two active regions. Nonetheless, data from the second group of Table 2 (days 22-53) show an increment in the separation between the spots of only 0.02 phases and practically no sporadic flares. This change happened without a clear counterpart neither in the photometry, nor in the basal chromospheric emission.

## 6. Summary and conclusions

We have analyzed four months of quasi-simultaneous spectroscopic and photometric observations of the young K2 dwarf LQ Hya to study the connection between photospheric spots and chromospheric active regions, as well as the evolution of the activity in the short term.

The Doppler maps show that the stellar surface was dominated by three spots; a low-latitude spot (S1) and two bigger spots at higher latitudes (S2 and S3). The three spots are present in all maps, indicating that the active regions of LQ Hya can live for at least four month. The combined use of the  $V$ -band photometry and the Doppler maps reveal that the changes in the photosphere of the star were mostly a consequence of the spatial redistribution of the spots. The photometric light curve presents clear rotational modulation with minimum brightness at the midpoint between S2 and S3. As the spots moved apart from each other the amplitude of the modulation decreased from  $0^m16$  at the middle of the observations to  $0^m09$  at the end. These process took place while the mean brightness of the star remained constant at a value of  $V \approx 7.90$  mag.

The chromospheric emission shows a good anti-correlation with the photometric light curve, but also some differences. The side of the star with highest emission was centered at the midpoint between the spots S2 and S3, and moved toward higher phases with them. Curiously, the basal emission from that side of the star remained constant while S2 and S3 move apart from each other instead of declining in anti-correlation with the brightness. The study of the  $H\alpha$  and  $H\beta$  lines as the star rotates reveals the coexistence of chromospheric active regions and photospheric dark spots. The chromospheric emission associated to the spots S2 and S3 remained roughly constant but increased for the spots S1. This led to an overall increment of the chromospheric basal emission that seems to be somewhat disconnected from the photosphere. Additionally, the asymmetries at the core of the  $H\alpha$  line suggest the existence of a radial outflow surrounding the spots.

We also detected higher flare activity during the first twenty days of observations. One of the flares produced an enhancement at the blue wing of the  $H\alpha$  line that lasted for more that two days. From the shape of the velocity profile and the lack of rotational modulation, we attributed the effect to a mass ejection.

*Acknowledgements.* We are grateful to the State of Brandenburg and the German federal ministry for education and research (BMBF) for their continuous support of the STELLA and APT activities. The STELLA facility is a collaboration of the AIP in Brandenburg with the IAC in Tenerife. We thank Lou Boyd for nursing the APTs at Fairborn Observatory, and Thomas Granzer for his help with the photometric data. Finally, we would also like to thank our anonymous referee for the helpful comments and suggestions.

## References

- Ambruster, C. & Fekel, F. 1990, in BAAS, Vol. 22, 857
- Bein, B. M., Berkebile-Stoiser, S., Veronig, A. M., et al. 2011, ApJ, 738, 191
- Berdyugina, S. V., Ilyin, I., & Tuominen, I. 2001, in Astronomical Society of the Pacific Conference Series, Vol. 223, 11th Cambridge Workshop on Cool Stars, Stellar Systems and the Sun, ed. R. J. Garcia Lopez, R. Rebolo, & M. R. Zapaterio Osorio, 1207
- Berdyugina, S. V., Pelt, J., & Tuominen, I. 2002, A&A, 394, 505
- Bidelman, W. P. 1981, AJ, 86, 553
- Cao, D.-t. & Gu, S.-h. 2014, AJ, 147, 38
- Cole, E. M., Hackman, T., Käpylä, M. J., et al. 2015, A&A, 581, A69
- Constable, S. C., Parker, R. L., & Constable, C. G. 1987, Geophysics, 52, 289
- Covino, S., Panzera, M. R., Tagliaferri, G., & Pallavicini, R. 2001, A&A, 371, 973
- deGroot-Hedlin, C. & Constable, S. 1990, Geophysics, 55, 1613
- Donati, J.-F. 1999, MNRAS, 302, 457

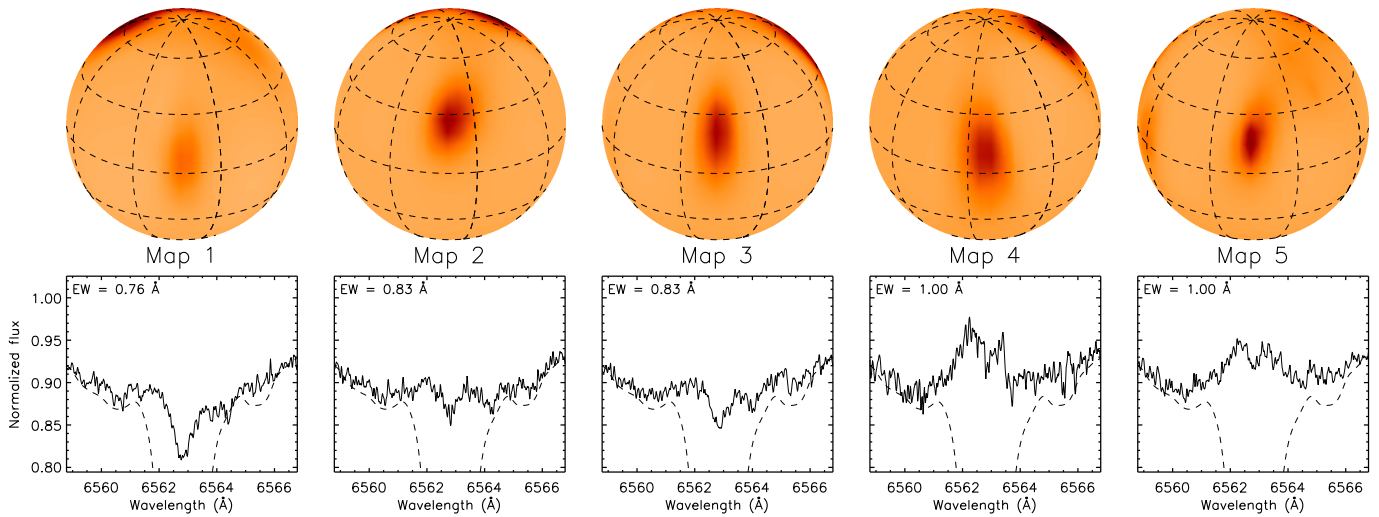


**Figure 11.** Orthographic projection of the five maps centered at the position of the spot S1 together with the average  $H\alpha$  line at that phase. The spectrum of the non-active reference star HD 3765 is shown as a dashed line. The color table is the same as in Fig. 5.

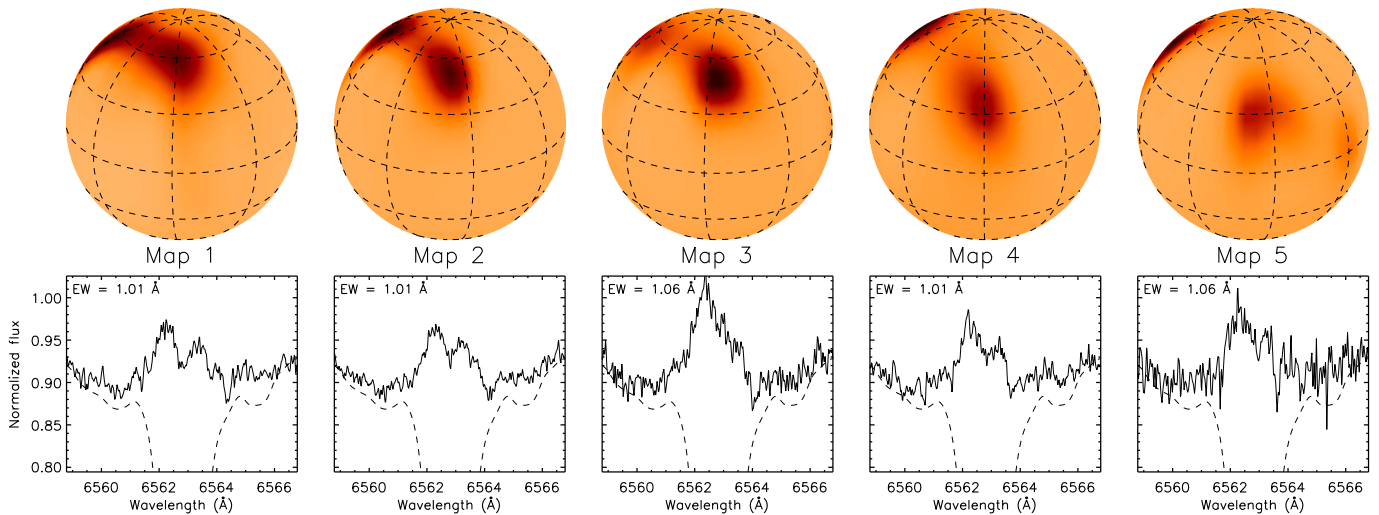


**Figure 12.** Same as Fig. 11 but for the spot S2.

- Donati, J.-F., Collier Cameron, A., Semel, M., et al. 2003, *MNRAS*, 345, 1145
- Doyle, J. G., Butler, C. J., Bryne, P. B., & van den Oord, G. H. J. 1988, *A&A*, 193, 229
- Doyle, J. G. & Byrne, P. B. 1987, in *Lecture Notes in Physics*, Berlin Springer Verlag, Vol. 291, *Cool Stars, Stellar Systems and the Sun*, ed. J. L. Linsky & R. E. Stencel, 173
- Eason, E. L. E., Giampapa, M. S., Radick, R. R., Worden, S. P., & Hege, E. K. 1992, *AJ*, 104, 1161
- Fekel, F. C., Bopp, B. W., Africano, J. L., et al. 1986a, *AJ*, 92, 1150
- Fekel, F. C., Moffett, T. J., & Henry, G. W. 1986b, *ApJS*, 60, 551
- Flores Soriano, M., Strassmeier, K. G., & Weber, M. 2015, *A&A*, 575, A57 (Paper I)
- Frasca, A., Kóvári, Z., Strassmeier, K. G., & Biazzo, K. 2008, *A&A*, 481, 229
- Gallagher, P. T., Lawrence, G. R., & Dennis, B. R. 2003, *ApJ*, 588, L53
- Granzter, T., Reegen, P., & Strassmeier, K. G. 2001, *Astronomische Nachrichten*, 322, 325
- Gray, D. F. 2008, *The Observation and Analysis of Stellar Photospheres* (Cambridge: Cambridge University Press)
- Gray, R. O. & Corbally, C. J. 1994, *AJ*, 107, 742
- Gunn, A. G., Doyle, J. G., Mathioudakis, M., Houdebine, E. R., & Avgoloupis, S. 1994, *A&A*, 285
- Hall, D. S., Kirkpatrick, J. D., & Seufert, E. R. 1986, *International Amateur-Professional Photoelectric Photometry Communications*, 25, 32
- Heintz, W. D. 1981, *ApJS*, 46, 247
- Houdebine, E. R., Foing, B. H., Doyle, J. G., & Rodono, M. 1993, *A&A*, 274, 245
- Houdebine, E. R., Foing, B. H., & Rodono, M. 1990, *A&A*, 238, 249
- Jetsu, L. 1993, *A&A*, 276, 345
- Kóvári, Z., Strassmeier, K. G., Granzer, T., et al. 2004, *A&A*, 417, 1047
- Kosovichev, A. G. & Zharkova, V. V. 1998, *Nature*, 393, 317
- Kurucz, R. 1993, *ATLAS9 Stellar Atmosphere Programs and 2 km/s grid*. Kurucz CD-ROM No. 13. Cambridge, Mass.: Smithsonian Astrophysical Observatory., 13
- Lehtinen, J., Jetsu, L., Hackman, T., Kajatkari, P., & Henry, G. W. 2012, *A&A*, 542, A38
- Lehtinen, J., Jetsu, L., Hackman, T., Kajatkari, P., & Henry, G. W. 2016, *A&A*, 588, A38
- Martínez González, M. J., Asensio Ramos, A., Carroll, T. A., et al. 2008, *A&A*, 486, 637
- Messina, S. & Guinan, E. F. 2003, *A&A*, 409, 1017
- Montes, D., Fernandez-Figueroa, M. J., de Castro, E., et al. 1998, in *Astronomical Society of the Pacific Conference Series*, Vol. 154, *Cool Stars, Stellar Systems, and the Sun*, ed. R. A. Donahue & J. A. Bookbinder, 1516
- Montes, D., Saar, S. H., Collier Cameron, A., & Unruh, Y. C. 1999, *MNRAS*, 305, 45
- Oláh, K., Kolláth, Z., Granzer, T., et al. 2009, *A&A*, 501, 703
- Oláh, K., Kolláth, Z., & Strassmeier, K. G. 2000, *A&A*, 356, 643
- Oláh, K. & Strassmeier, K. G. 2002, *Astronomische Nachrichten*, 323, 361
- Olsper, N., Käpylä, M. J., Pelt, J., et al. 2015, *A&A*, 577, A120
- Phillips, K. J. H., Bromage, G. E., Dufton, P. L., Keenan, F. P., & Kingston, A. E. 1988, *MNRAS*, 235, 573
- Rice, J. B. & Strassmeier, K. G. 1998, *A&A*, 336, 972
- Saar, S. H. & Bookbinder, J. A. 1998, in *Astronomical Society of the Pacific Conference Series*, Vol. 154, *Cool Stars, Stellar Systems, and the Sun*, ed.

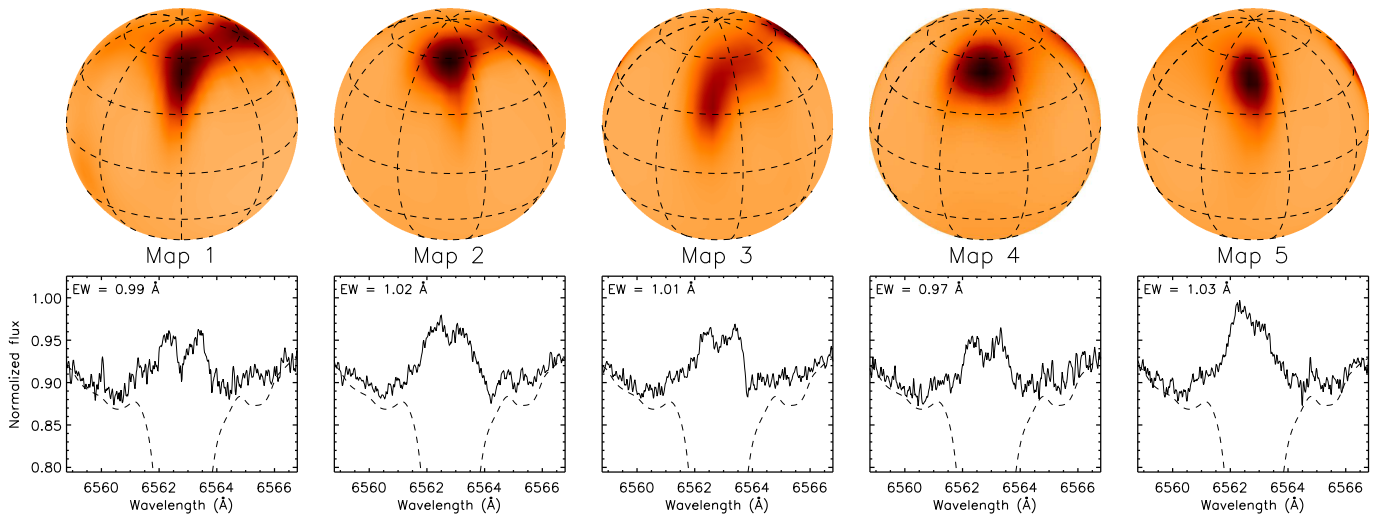


**Figure 13.** Same as Fig. 11 but for the spot S3.

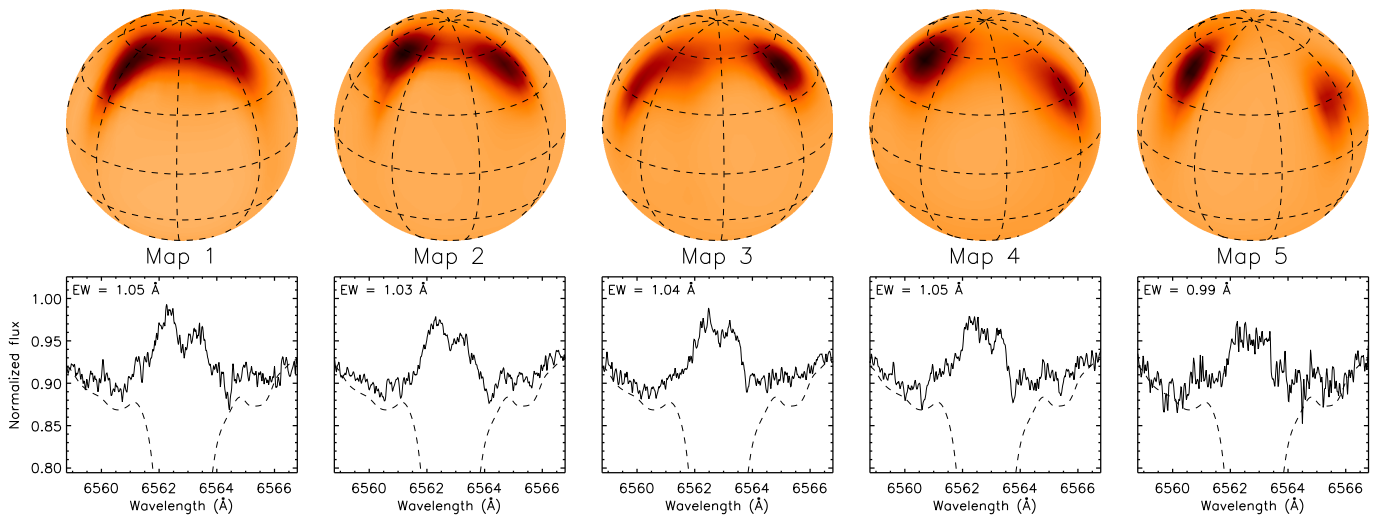


**Figure 14.** Same as Fig. 11 but for the midpoint between spots S2 and S3.

- R. A. Donahue & J. A. Bookbinder, 1560  
 Saar, S. H., Piskunov, N. E., & Tuominen, I. 1992, in *Astronomical Society of the Pacific Conference Series*, Vol. 26, *Cool Stars, Stellar Systems, and the Sun*, ed. M. S. Giampapa & J. A. Bookbinder, 255  
 Saar, S. H., Piskunov, N. E., & Tuominen, I. 1994, in *Astronomical Society of the Pacific Conference Series*, Vol. 64, *Cool Stars, Stellar Systems, and the Sun*, ed. J.-P. Caillault, 661  
 Strassmeier, K. G., Bartus, J., Cutispoto, G., & Rodono, M. 1997a, *A&AS*, 125, 11  
 Strassmeier, K. G., Boyd, L. J., Epan, D. H., & Granzer, T. 1997b, *PASP*, 109, 697  
 Strassmeier, K. G., Granzer, T., Weber, M., et al. 2010, *Advances in Astronomy*, 2010  
 Strassmeier, K. G., Rice, J. B., Wehlau, W. H., Hill, G. M., & Matthews, J. M. 1993, *A&A*, 268, 671  
 Venkatakrishnan, P., Kumar, B., & Uddin, W. 2008, *MNRAS*, 387, L69  
 Wöhl, H. & Brajša, R. 2001, *Sol. Phys.*, 198, 57

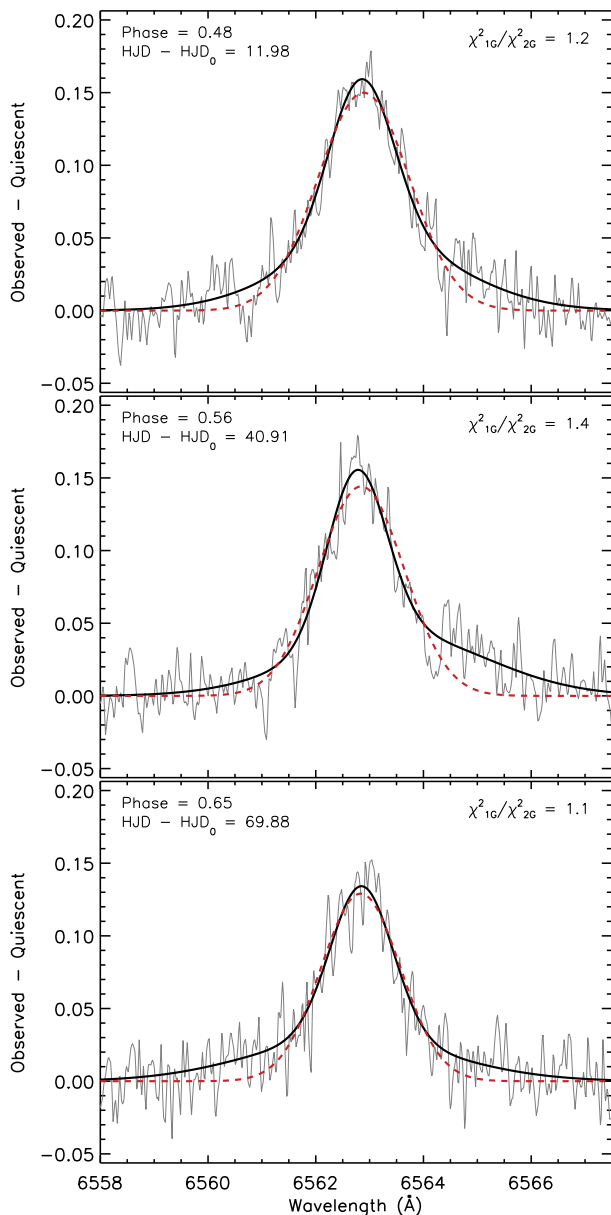


**Figure A.1.** Example of three subtracted  $H\alpha$  lines showing broad wings despite their relatively low emission. The EW of the net emission profiles is between 1.0 and 1.1 Å. The subtracted profiles and their corresponding 1- and 2-Gaussian fits are shown as a gray thin, solid black, and dashed red line, respectively. The ratio of the chi-square goodness of the fits is indicated on the right side of each panel.

### Appendix A: Example $H\alpha$ lines with broad wings and relatively low emission

Roughly a half of the  $H\alpha$  lines from the basal emission with EWs in the range 1.0-1.1 Å show broad wings that could be a consequence of micro-flare activity. Fig. A.1 shows a few examples.

### Appendix B: Observed and inverted line profiles.

Figure B.1 shows the average profiles of the 19 individual lines used for Doppler imaging, together with the averaged inverted lines. The rotational phase and the date of each spectrum are also indicated.

### Appendix C: Example of map affected by distorted lines

Spectral lines affected by high levels of noise, or distorted by activity phenomena other than spots, can produce spurious features in the Doppler maps. In Fig. C.1 we show as an example the effect that seven spectra affected by a possible mass ejection have on the first map of Fig. 5.

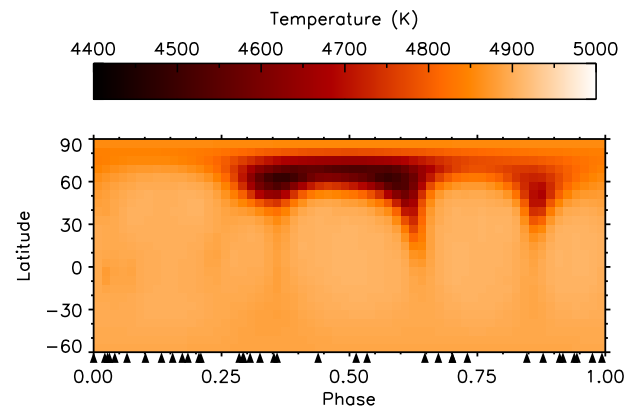


**Figure C.1.** Doppler map computed in the same manner as the first map in Fig. 5, but including seven spectra affected by a possible mass ejection from a flare. As a result of this, the near equatorial spot from phase 0.1 disappears, the resolution at high latitudes get worse, and an artifact near phase 0.85 appears.

### Appendix D: Example of the effect of telluric lines on the red peak of the $H\alpha$ line

In Fig. D.1 we simulate an  $H\alpha$  profile dominated by a red peak reversing the  $H\alpha$  line of Fig. 8 and phase 0.4. To simulate the effect of telluric lines in a worst case scenario we chose a template with telluric lines slightly stronger than in any LQ Hya spectrum. The template was shifted to match the closest distance between the strongest telluric line and the red peak compatible with the observations.

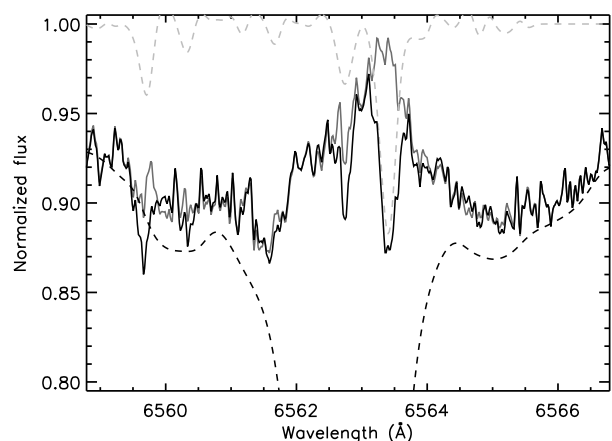


**Figure D.1.** Simulated effect of telluric lines on the red peak of the  $H\alpha$  line in a worst case scenario. The black-solid line is the result of multiplying the gray-solid line with the telluric template (gray dashed). The non-active reference spectrum of HD 3765 is shown as a black-dashed line.

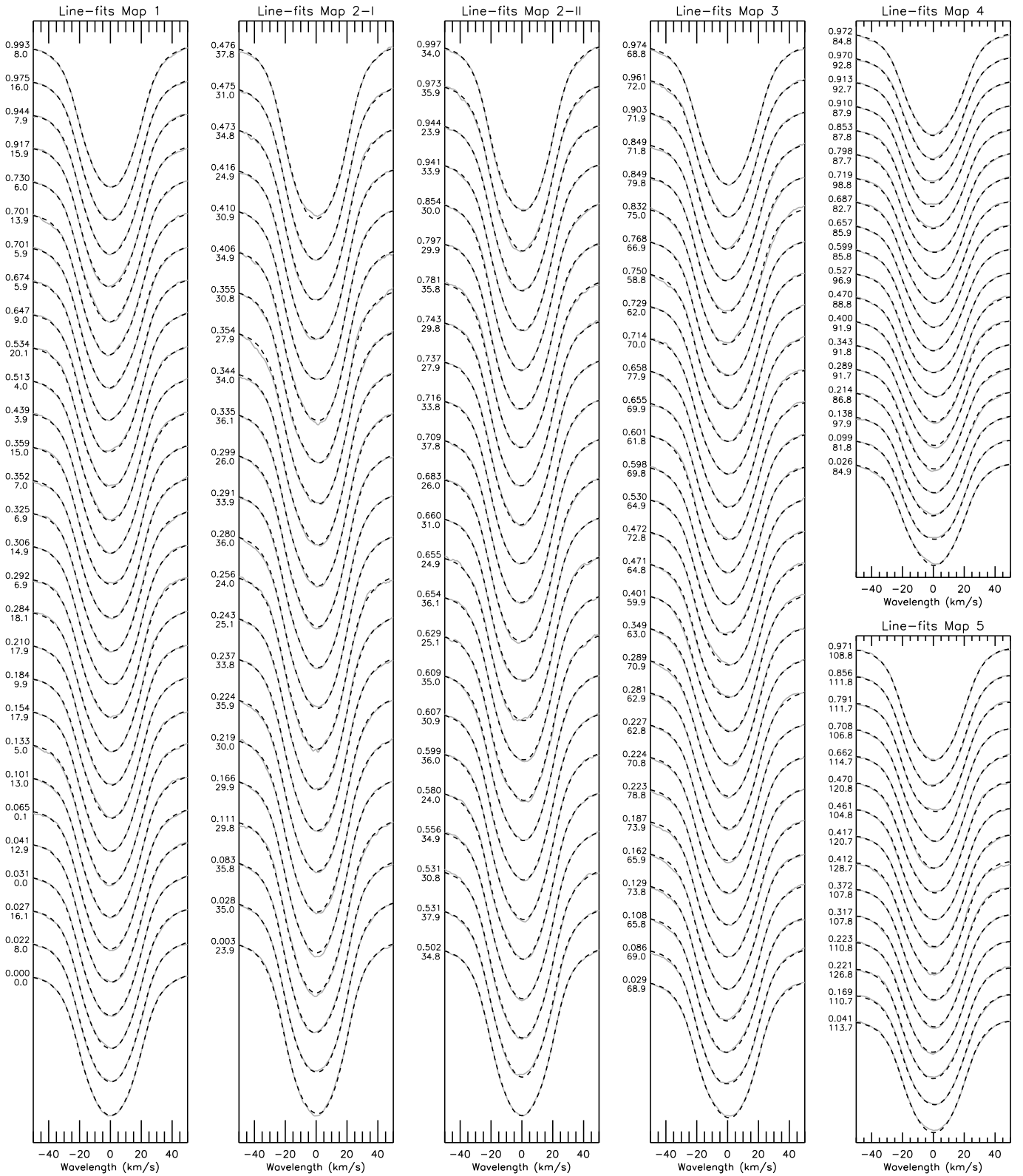


**Figure B.1.** Average line profiles used for the inversion (gray solid) together with their model fit (black dashed). The two numbers on the left side of each line indicate the rotational phase (top) and the relative time  $HJD - HJD_0$  (bottom).